Investigating the Performance of Electrical Resistivity Arrays

Lee J. Perren

Thesis submitted to the Faculty of the
Virginia Polytechnic Institute and State University
in partial fulfillment of the
requirements for the degree of

Master of Science
in
Geophysics

Dr. John A. Hole, Chair

Dr. J. Arthur Snoke

Dr. Matthis G. Imhof

September 9, 2005

Blacksburg, Virginia

Keywords: Exploration Geophysics, Electrical Resistivity, Array Performance, Boundary Reproduction

Investigating the Performance of Electrical Resistivity Arrays

Lee J. Perren

Abstract

2D inversion modeling of synthetic data is used to evaluate the performance of five electrical resistivity arrays, with the primary criteria being the reproduction of sharp model boundaries. 2D synthetic noise free data were calculated simulating a modern fixed spacing multi-electrode cable. Twelve 2D synthetic models, resembling a number of different geologic situations, were used to investigate performance of the dipole-dipole, pole-dipole, pole-pole, Wenner and Schlumberger arrays

Although the synthetic, noise-free data were well matched for all inversions, many of the inversion results exhibit substantial mismatches from the true model. The greatest resistivity mismatches are near model discontinuities. Resistivity mismatches become worse with depth and the geometry of geologic boundaries in the deep portion of the models are not well reproduced by any of the arrays. Field surveys must be designed so that the geologic target is in the middle of the data constrained region. Different arrays performed best for different models and a practical table is presented allowing the practitioner to choose the optimal array for the particular geologic situation under investigation. Although the dipole-dipole and pole-dipole arrays may not be the optimal array for a given geology, they rarely fail for any model, and thus are recommended for reconnaissance or preliminary investigations in regions of unknown geology.

Contrary to traditional advice found in textbooks, based on 1D profiling and sounding, and data plot comparison, this study, using 2D data and 2D inversion, finds the Wenner and Schlumberger arrays, thought to perform poorly for vertical boundaries, performed well for a vertical boundary and a thin vertical resistor. Similarly, the dipole-dipole and pole-dipole arrays, thought to perform poorly for horizontal and dipping boundaries, performed well for several models containing those geometries. Another interesting finding is that changing the polarity of geologic units from resistors to conductors changed relative array performance in most models.

Acknowledgments

I would like to sincerely thank everyone who has helped me in my journey to completion of this thesis. Thanks to the Department of Geosciences for continuing to support me with office space, a computer, supplies and every other tool I needed to finish this work. Thanks to the entire faculty of the department for their instruction and guidance. Thanks to the wonderful support staff: Connie Lowe, Ellen Mathena, Richard Godbee, Carolyn Williams, Linda Bland, Mary McMurray, and everyone else who keeps this place running like a well oiled machine. We could not do any of this without you!

I would like to thank my committee members Dr. John A. Hole, Dr. Matthias G. Imhof, and Dr. J. Arthur Snoke, for their comments and criticisms that made this thesis a better product. I would especially like to thank Dr. John Hole for continuing to advise, support and encourage me through this process. Thanks to Dr. Tom Burbey for the use of the software dongle that allowed for full access to the capabilities of RES2DMOD and RES2DINV.

I would like to thank my family whose support and encouragement helped keep me focused and have carried me through this process. To my friends and fellow graduate students, I thank you for your friendship, especially my fellow “hard timers” whose Saturday night gatherings kept me sane.

A very special thank you to Alanna Lester who believed in me, encouraged me, and has inspired me to be the best person I can. Thank you so much for your friendship.

Thanks to you all!!!!

Table of Contents

List of Tables

List of Figures

List of Appendices

Introduction

Direct current resistivity (DCR) is a shallow geophysical imaging technique for the upper few hundred meters of the earth that combines ease of use with affordable equipment, making it a very appealing technique for a variety of different fields including environmental, geotechnical and civil engineering, mining, hydrogeology, and archeology. These very different applications require choosing the DCR electrode array that is best suited to resolve the geologic situation under investigation. The goal of this research is to evaluate the performance of five, common, commercially used DCR electrode arrays with respect to their ability to resolve geologic structures.

Resistivity surveying began in the 1920's, and the tools to collect resistivity data changed very little through the early 1980's. Field studies completed during this period were time and labor intensive. The original design had four electrodes inserted into the ground and attached by individual cables to an ammeter (current), an electric power source and a voltmeter (potential). DCR data were collected by measuring the spacing between electrodes, the current applied at two electrodes, and the potential between the two remaining electrodes. The information for one measurement was recorded, some or all of the four long cables and electrodes were moved to new locations, and the procedure repeated. Following this procedure, tens of measurements could be collected in an average workday. Different relative positions and spacing of current and potential electrodes (arrays) were used, with the most common being the dipole-dipole, the pole-dipole, the pole-pole, the Wenner and the Schlumberger arrays (Figure 1) [e.g., Telford, 1990; Reynolds, 1997; Sharma, 1997]. An important criterion defining these arrays was

ease of field operation, often more so than imaging capabilities, [e.g., Telford, 1990; Reynolds, 1997].

The data are expressed as an apparent resistivity plotted at the array midpoint and a pseudodepth, Figure 2. Apparent resistivity is the voltage to current ratio, scaled by an array geometry factor that assumes a homogeneous earth model [e.g., Telford, 1990]. Pseudodepth approximates in the homogeneous earth model the depth at which half of the current density is from above and half is from below [Edwards, 1977]. Laboratory analysis of data relied on graphical matching of master curves for simple geologic models and very general interpretations until the common availability and use of computers in the 1970's, [Telford, 1990; Reynolds, 1997]. Field equipment and computing technology limitations controlled research, and as a result, mostly 1D data were collected or modeled as either horizontal profiles or vertical soundings. Horizontal profiles are composed of data collected with fixed array spacing. The data for the initial position is recorded; the array is moved one electrode spacing and the data for the new position is recorded. This procedure is repeated multiple times until a series of data points (profile) is recorded. Vertical soundings are composed of data collected with the array spacing expanding about the midpoint of the array for successive measurements. The expansion is repeated multiple times until a series of data points (sounding) is recorded. During this time, relative array performance was evaluated by comparing the shapes and maximum values of the data profiles or soundings recorded for each array, [Coggon, 1973; Ward, 1990 and references included therein].

Studies of the performance of standard electrode arrays for various geologic situations have resulted in conventions and tables of applicability of each array [e.g., Roy

and Apparao, 1971; Coggon, 1973; Dey et al, 1975; Edwards, 1977; Ward, 1990; Telford, 1990; Reynolds, 1997; Sharma, 1997]. These conventions and tables were derived based upon time and labor-intensive four-electrode field equipment, 1D horizontal profiles or vertical soundings, and semi-quantitative data analysis based on master curve fitting or trial and error pseudosection matching. Ward (1990) reviewed research of array performance and stated that the dipole-dipole array appears best suited for lateral location of vertical boundaries, followed by the pole-dipole, Schlumberger, and finally Wenner arrays. For resolution of dipping structures and horizontal layers, the ranking of arrays from best to worse is: Schlumberger, Wenner, dipole-dipole, and pole-dipole. We here call these performance evaluations "conventional wisdom" because they are widely available and commonly are the basis of array choice for modern usage [e.g. Telford, 1990; Reynolds, 1997; Sharma, 1997].

Since the mid-1980's, there has been a continuous evolution in the acquisition, interpretation, and inversion of DCR data. During the late 1980's and early 1990's, computer controlled multi-electrode systems became widely available [e.g., Griffiths & Turnbull, 1985; Griffiths et al., 1990; Griffiths & Barker, 1993]. These systems use a single multi-cored cable with electrode takeout positions at regularly spaced intervals, which is deployed and left in a fixed position while a computer controls data acquisition. This setup allows up to several hundred electrodes to be attached to a recording system, where a computer-controlled switch changes the combination and spacing of current and potential electrodes based on a user defined parameter file. Many of these systems are single-channel, allowing collection of only one apparent resistivity at a time. Recently, multi-channel systems have become available allowing collection of multiple apparent

resistivities at the same time for a given current electrode pair. These multi-electrode and multi-channel systems greatly decreased field time and labor necessary to carry out large 2D and 3D studies and enabled hundreds to thousands of measurements to be collected in hours. Concurrent with these improvements in field data acquisition, improvements in computer technology allowed 2D and 3D forward and inversion modeling to become the primary methods for interpreting resistivity data, [e.g., Loke & Barker, 1995; Loke & Barker, 1996; Li & Oldenburg, 2000; Loke et al, 2003; Stummer et al., 2004].

The equipment, analysis methods, and computing power used to collect, process, model, and interpret resistivity data have improved greatly over the last twenty years. Therefore, array performance needs to be re-evaluated for the current tools. The multi-electrode multi-cored cable systems allow collection of 2D data by simultaneously sounding and profiling. 2D inversion of the data collected with these multi-electrode systems is the common method of data analysis. In practice it is still common to use the conventional wisdom to determine the appropriate array. Array choice for modern 2D studies are then based upon the conventions derived from 1D studies and semi-quantitative dataanalysis based on master curve fitting or trial and error pseudosection matching. 1D and 2D data are significantly different and sharp, strong signatures in 1D apparent resistivity data plots can not be compared to 2D subsurface resistivity models. As we show below, conventions derived from 1D data and curve matching may not apply to 2D data and inversion analysis.

Seaton and Burbey, 2002, qualitatively evaluated DCR array performance for geologically complex 2D models and concluded that the Wenner and Schlumberger arrays revealed less detail than the dipole-dipole array and that the pole-pole array had

the poorest resolution. Dahlin and Zhou, 2004, quantitatively evaluated DCR array performance for geologically complex 2D models using cross-correlation methods and concluded that the gradient, pole-dipole, dipole-dipole, and Schlumberger arrays are strongly recommended for 2-D resistivity imaging. They also concluded that the final choice of DCR array should be determined by the expected geology with the gradient array particularly recommended for multi-channel systems and production of images comparable to ones for the pole-dipole and dipole-dipole arrays. The pole-dipole array is recommended for good spatial resolution, the dipole-dipole array for vertical and dipping structures, and the Schlumberger array for good depth determination. To better exploit the capabilities of multi-electrode acquisition systems, Stummer et al., (2004) investigated selection of optimized electrode combinations in non-standard array geometries based on their sensitivity to changes in subsurface parameters. They concluded that more geologic information was provided by the optimized data sets when compared to standard array data sets of equal size.

In previous synthetic modeling studies (e.g. Seaton & Burbey, 2000; Dahlin & Zhou, 2004, Stummer et al., 2004), relative array performance has been evaluated by qualitative assessment of inversion model or by a single statistic comparing the inversion result to the true resistivity model, such as root mean square (RMS) of the mismatch, or cross correlation between the true model and the inversion result. Important attributes of the inversion results in the applied use of DCR are the position and width of boundaries, which are not well evaluated by these assessment methods. Single statistics do not reveal the location of mismatches in the model or distinguish between mismatches in the magnitude of resistivity within geologic units and mismatches in the position of

boundaries between geologic units. DCR surveys are commonly used to determine the geometry of geologic structures; however, very little research has focused on quantitative evaluation of array performance at reproducing model geometries.

This study quantitatively evaluates the performance of five common, commercially used arrays at reproducing model geometries. Synthetic data are computed simulating a modern 50-electrode system for twelve simple 2D geologic models using the dipole-dipole, pole-dipole, pole-pole, Wenner and Schlumberger arrays. 2D inversion models are obtained from the data for each array-model combination using common, commercially used software. Model mismatch as a function of depth is calculated with the prime criteria for array performance being resistivity boundary reproduction.

Method

Forward Modeling

The synthetic models were designed to be generic and simple (Figure 3), yet represent multiple geologic possibilities (Table 1). The resistivities of geologic units in the models are 100 and 1000 Ω-m. This order of magnitude difference represents typical contrasts encountered in earth materials.

Synthetic data were computed for 12 simple 2D geologic models using RES2DMOD ver. 3.01q, (Loke & Barker, 1996), because it is a widely available and common, commercially used forward-modeling program. This program uses a gridded finite difference algorithm to solve for the 2D apparent resistivities (Loke & Barker, 1996).

Noise free data sets were computed for a simulated line with 50 fixed electrodes, which represents a typical number of electrodes in a common commercial cable. Noise is

an issue for field data, however stacking data or increasing the electric current can increase the signal-to-noise ratio. Noise in the data may decrease the resolution of resulting images, but relative array performance should be similar. Electrode spacing of one unit was chosen to emphasize that the model could be scaled to other sizes with equivalent results. All of the models extended to 17.5 depth units. The finite difference grid layer thickness increased with depth because the spatial resolution of DCR decreases with depth. Layer thickness is constant within groups of four layers, with the groups having thicknesses of 0.25, 0.375, 0.5, 0.75, 1.0 and 1.5 units for a total of 24 layers (Figure 2). The models were parameterized with four model blocks between neighboring electrodes. This results in 196 blocks per layer and 4704 total blocks in the model.

The difference between the five arrays tested in this study is the arrangement and spacing of electrodes. For this study, the Wenner (WN), Schlumberger (SC), and dipole-dipole (DD) arrays are referred to as "four-pole arrays", the pole-dipole (PD) as a "three-pole array" and the pole-pole (PP) as a "two-pole array". The WN and SC arrays have the potential electrodes (v) between the current electrodes (i); for this study these arrays are referred to as "inside arrays". These arrays were designed for vertical sounding and are conventionally thought to be the optimal arrays for resolving horizontal boundaries [e.g. Ward, 1990; Telford, 1990; Reynolds, 1997]. The DD, PD, and PP arrays have the potential electrodes outside of the current electrodes; for this study these arrays are referred to as "outside arrays". These arrays were designed for horizontal profiling and are conventionally thought to be the optimal arrays for resolving vertical boundaries [e.g. Ward, 1990; Telford, 1990; Reynolds, 1997].

The electrodes for each array are spaced a particular distance apart as defined by the *a* and *n* variables in Figure 1, referred to as the *a*- and *n*-spacings. Whole number increments of *a*-spacings, starting at 1 and increasing up to the maximum of 16, were used to calculate the forward-modeled responses for all arrays (Table 2). Whole number increments of *n*-spacings, starting at 1 and increasing up to 6, were used for the DD, PD, and SC (Table 2). These *a*- and *n*-spacings are typical commercially used values and are restricted to whole numbers because the spacing between electrodes is fixed. The maximum number of data points were calculated for each array using all possible combinations of the *a*- and *n*-spacings (Table 2). The number of data points for each array is very different and is an inherent limitation of each array in fixed cable systems. For each array, the combinations of *a*- and *n*-spacings result in different pseudodepths and midpoints, which provide an indication of good and poor data coverage in density and spatial distribution (Figure 2). The minimum and maximum pseudodepths for each array tested are shown in Table 2.

Inverse Modeling

2D inversion modeling was carried out using RES2DINV ver. 3.51z, (Loke & Barker, 1996), because it is a widely available and common, commercially used inversion program. The inversion routines used by the program are based on the Gauss-Newton, smoothness-constrained, least-squares method for L_2-norm optimization (Loki & Barker, 1996) and the smoothness-constrained, iteratively reweighted least-squares method for L_1-norm optimization (Loke et al., 2003). The default method in the program is L_2-norm optimization, which creates inversion results with smooth variations in resistivity and is a good optimization choice when gradual changes are expected in the geology. The L_1-

norm optimization method allows models with sharper variations in resistivity and is a better optimization choice when geological discontinuities are expected (Seaton & Burbey, 2002; Loki et al, 2003; Dahlin & Zhou, 2004). The L_1-norm optimization method was chosen in this study because the goal was reproduction of sharp geologic boundaries.

Most of the RES2DINV default inversion parameters were used for consistency between arrays and models. This is also consistent with what many commercial practitioners would choose. Altering the inversion parameters may have changed the resolution of each model, but relative array performance should not change significantly. A complete list of the RES2DINV inversion parameters is included in Appendix A.

The number of layers and layer thicknesses in the inversion models were chosen to match those in the true resistivity models. The inversion models were parameterized with one model block between neighboring electrodes, resulting in 49 blocks per layer and 1176 total blocks in the model (Figure 2). Resistivity boundaries between geologic units in the forward models are placed between model blocks. In choosing matching locations and sizes of forward and inversion model blocks, this study is forcing the inversion model boundary to be between blocks. In reality, boundaries will likely fall within inversion model blocks. If modeling had been carried out with boundaries within blocks the resolution might have changed, but relative array performance should be the same because the models are oversampled and smoothed.

Data Analysis

In order to compare the true model (4704 blocks) to the inversion result (1176 blocks), each layer in the true model was horizontally resampled to one fourth of the

original. Subsurface data coverage is poor in the bottom corners of the models as indicated by the pseudodepths and midpoints of Figure 2. Therefore, these corners were truncated to the region of data coverage from the PP array, the array with the widest coverage, prior to performance evaluation.

A first indicator of a model's quality is the misfit between the observed and calculated data, usually a single value for the entire data set. A reasonably small misfit is a necessary condition to accept the model as a close approximation to subsurface geology. However, non-linear inversion, inverse solutions are in general non-unique, and a small data misfit does not mean that the model mismatch is small. A common method in synthetic modeling research to evaluate a model is to look at the mismatch between the true model and inversion result. Usually a single cumulative statistic is used, such as RMS of the difference in resistivity or cross correlation of resistivity across the entire model. A single statistic cannot determine the location of mismatches in the model nor distinguish between mismatches in the magnitude of resistivity within geologic units and mismatches in the position and width of boundaries between geologic units.

To address the issue of location of mismatch within the model, the RMS of the percent difference in resistivity between the true model and inversion result was calculated for each layer of the model using the following equation,

$$layerRMS = \sqrt{\frac{1}{N}\sum_{i=1}^{N}\left(\frac{\rho a_i - \rho at_i}{\rho at_i} * 100\right)^2}$$

where ρa_i is the apparent resistivity of the ith block of the layer in the inversion result, ρat_i is the apparent resistivity of the ith block of the layer in the true model, and N is the number of blocks in the layer. Percent differences were used to normalize values because

resistivities can vary by orders of magnitude. Layer-by-layer model mismatches were calculated and plotted at the depth of the midpoint of that layer. RMS mismatches were also calculated for overlapping shallow, intermediate-depth, and deep portions of the model (Figure 2). Performance of each array for the three depth ranges was assigned a letter grade based on the RMS mismatch using the following scheme; "A" < 20%; "B" 20-40%; "C" 40-60%; "D" 60-80%; "E" >80%. "A" and "B" indicate good array performance, "C" indicates acceptable array performance, "D" and "E" indicate poor array performance for the model. An overall array performance grade is calculated by grade point averaging of the three layers for each array.

The layer-by-layer mismatches best show array performance as a function of depth. However, these statistics do not distinguish between mismatches in the magnitude of resistivity within geologic units or mismatches in the position of boundaries between geologic units.

Maximum values of the 2D spatial gradient of the inversion result calculated using finite differences were used to indicate the positions of boundaries between geologic units. The boundary was considered "not found" if the maximum value was not above the standard deviation for the layer or less than 90 ohms (10% of the difference between geologic units). These criteria were implemented to avoid choosing values in layers where there is no boundary or where minor fluctuations in resistivity values may be interpreted as maximums. Mean mismatches between the positions of vertical and dipping boundaries in the true model and inversion result were calculated using the following equation,

$$\frac{1}{N}\sum_{i=1}^{N}\left|\frac{bp_i - bpt_i}{bpm_i}\right|$$

where bp_i is the boundary position in the ith row of the inversion result, bpt_i is the boundary position in the ith row of the true model, bpm_i is the distance between the boundary position and the model edge in the ith row of the true model, and N is the number of rows. For horizontal boundaries the same equation was used exchanging rows with columns. These mismatches were normalized, as a percent of the maximum distance from the true boundary to the model edge, for the shallow, intermediate-depth and deep portions of the models. Normalization was performed to ensure grading consistency for each array and from model to model. Performance of each array was assigned a letter grade for the three depth ranges based on the mean position mismatch by the following scheme; "A"< 5%; "B" 5-10%; "C" 10-15%; "D" 15-20%; "E" >20%. "A" and "B" indicate good array performance, "C" indicates acceptable array performance, "D" and "E" indicate poor array performance for the model.

Maximum values of the 2D spatial Laplacian calculated using finite differences were used to assess width or sharpness of the boundary between geologic units. The boundary edge was considered "not found" using the same criteria as the boundary position. The distances between points of inflection were used to indicate boundary width. Mean mismatches between the widths of vertical and dipping boundaries in the true model and inversion result were calculated using the following equation,

$$\frac{1}{N}\sum_{i=1}^{N}\left|\frac{bw_i - bwt_i}{bwm_i}\right|$$

where bw_i is the boundary width in the ith row of the inversion result, bwt_i is the boundary width in the ith row of the true model, bwm_i is the combined distance between the boundary edges and the model edges in the ith row of the true model, and N is the

number of rows. For horizontal boundaries the same equation was used exchanging rows with columns. These mismatches were normalized, as a percent of the maximum distances from the true boundary edges to the model edges, for the shallow, intermediate-depth and deep portions of the models. Normalization was performed to ensure grading consistency for each array and from model to model. Performance of each array was assigned a letter grade for the three depth ranges based on the mean width mismatch using the same scheme as the position mismatch.

For practical application, simultaneous determination of position and sharpness of boundaries is important. Therefore, a combined mismatch was calculated, by summing the mean mismatches in boundary position and width for the shallow, intermediate-depth, and deep portions of the model. Performance of each array was assigned a letter grade for the three depth ranges based on the combined mismatch using the same scale as the position mismatch. An overall array performance grade for boundary reproduction was calculated by grade point averaging of the three layers for each array. This overall array performance grade is used to define relative array performance.

Results - Vertical Boundary Model

There are twelve geologic models and five arrays for each model. We discuss only the results from the vertical boundary model (Figure 1) here. The results for all twelve models are included in appendices and a summary of the results is presented in the discussion sections.

Figure 4 shows that all of the inversions located the vertical boundary within the model but the position and width of the boundary varies from array to array.

Resistivity Mismatch

Table 3 shows the RMS data misfit, the RMS model mismatch and the array ranking based on the RMS model mismatch in numerical order from 1st to 5th. Data misfits are calculated in RES2DINV as the RMS of the percent difference between the observed and calculated apparent resistivities. The dimensions and normalization are the same for the data misfit and model mismatch allowing direct comparison. The average model mismatch is 86 times the average data misfit. This emphasizes that the inversion model does not necessarily represent the subsurface with the same degree of accuracy as the data misfit.

The graph of the layer-by-layer resistivity mismatch for the vertical boundary model (Figure 5) shows that all arrays perform well in the shallow portion of the model. The resistivity mismatch for all arrays begins in the intermediate-depth portion of the model and gets progressively worse with depth, as expected. The SC array performs best for most of the intermediate-depth, which contradicts conventional wisdom since the inside arrays are thought to be worse for vertical layers. The good performance of the SC array is also contrary to the single statistic model mismatch (Table 3) that ranks the SC array as 3rd best. The DD array performs the best at greatest depth.

Table 4 shows the resistivity mismatch and array performance grade for the shallow, intermediate-depth, and deep portions of the model and the overall array performance grade for each array. All arrays score A's in the shallow and intermediate-depth portion of the model. For the deep portion of the model the DD array scores an A, the PD, PP and SC arrays score B's, while the WN scores a C. The overall array performance grades show good and similar performance for the DD, PD, PP and SC,

closely followed by the WN. All arrays perform well in matching model resistivities. The good performance of the inside arrays contradicts conventional wisdom that inside arrays are worse for vertical boundaries.

Boundary Mismatch

Figure 6 shows the 2D spatial gradient and 2D spatial Laplacian calculated from the inversion results shown in Figure 4. These plots show that all inversions located the boundary within the model but the position and width of the boundary varies from array to array. Table 5 shows the mean normalized mismatch of the boundary position and array performance grades for the shallow, intermediate-depth and deep portions of the vertical boundary model. All arrays score A's in the shallow and intermediate-depth portion of the vertical boundary model. The DD, WN and SC arrays score A's for the deep portion of the model while the PD and PP score a B and C, respectively.

Table 6 shows the mean normalized mismatch of the boundary width and array performance grades for the shallow, intermediate-depth and deep portions of the vertical boundary model. All arrays score A's in the shallow and intermediate-depth portion of the model. The DD, WN and SC arrays score A's for the deep portion of the model while the PD and PP score C's.

Table 7 shows the combined mean boundary mismatch and array performance grades for the shallow, intermediate-depth and deep portions of the vertical boundary model. All arrays score A's in the shallow and intermediate-depth portion of the model. The DD, WN and SC arrays score A's for the deep portion of the model while the PD and PP score C's.

Table 8 shows the overall array performance grades for the five arrays over the entire depth range of the vertical boundary model. The four-pole arrays (DD, WN and SC) perform equally, with all arrays receiving A's. The PD and PP arrays perform equally well, with both arrays receiving B's. Since multiple arrays receive the same overall performance grade, the relative differences seen on the gradient and Laplacian plots, and the number of data points for each array are possible criteria for separating the arrays.

The gradient and Laplacian plots in Figure 6 show that there are differences in both the magnitude of the gradient and width of the boundary (Laplacian). The magnitude of the gradient is greatest for the SC, followed by the DD, and finally the WN array. The DD and WN arrays resolve the boundary wider at depth than the SC array. Using this information as a secondary criterion, the relative ranking of these arrays would be: 1st-SC (best), 2nd-DD, and 3rd-WN (worse).

However, from a practical standpoint, important factors are the time it takes to collect data in the field and carry out inversions of the data, both of which are linked to the number of data points collected. Therefore, an alternate criterion might be the number of data points necessary to obtain the results. Table 2 shows the number of data points for each array using the standard *a*- and *n*-spacings. Normalizing the number of data points to the WN array, which has the fewest data points, shows that the PP array takes 1.7 times longer to collect, the SC 2.7 times, the DD 3.5 times and the PD 4.5 times. Using the fewest data points necessary to obtain similar results as a secondary criterion, the relative ranking of the arrays would be: 1st-WN, 2nd-SC, and 3rd-DD.

Relative array ranking using either secondary criterion ranks an inside array's performance as the best. These rankings contradict the conventional wisdom that inside arrays are worse for resolving vertical boundaries.

For the purpose of this study the primary criteria for array grade is the combined mismatch, which is based on the reproduction of boundary position and width. When two or more arrays receive the same grade, the practitioner should decide whether field and inversion time (number of data points) or a slightly better fit in position and width of geologic boundaries is the more important criterion.

Results - All models

The graphs of the resistivity mismatch as a function of depth for all twelve models are included as Appendix B. Tables of the resistivity mismatch and array performance grades for the shallow, intermediate-depth, and deep portions of the models, and overall array performance grades for all array-model combinations are included in Appendix C. The overall array performance grades for all twelve models based on the resistivity mismatches are shown in Table 9.

Inversion results for all twelve models are included in Appendix D. Plots of the 2D spatial gradient and 2D spatial Laplacian of the inversion results for all array-model combinations are included in Appendix E. Tables of combined boundary mismatch and array performance grades for the shallow, intermediate-depth, and deep portions of the model, and overall array performance grades for all array-model combinations are included in Appendix F. The overall array performance grades for all twelve models based on combined boundary position and width mismatches of geologic boundaries are shown in Table 10.

Tables 9 and 10, the overall array performance grades, are the primary contributions of this work. They may be used to replace conventional array performance tables, based on 1D data and analysis, found in exploration geophysics texts.

Discussion

Resistivity Mismatch

The inversion code computes one model, the L_1-norm optimization best-fit model, out of an infinite number of models that fit the data. For all twelve models, although RMS data misfits averaged below 1%, RMS model mismatches averaged 48% (Appendix G). This emphasizes that a close fit to the data does not necessarily mean that the inversion result matches the true earth model with the same degree of accuracy. Similarly, Li & Oldenburg (2000) show three distinctly different models, derived from the same data with different optimization methods, which have the same data misfit. Since the data misfit is the only criterion available for real data, practitioners need to be careful interpreting how well the inversion model represents the subsurface.

The resistivity mismatches (Table 4 for the VB model and Appendix C for the remaining models) show that for the vertical boundary (VB) and vertical resistor (VLH) models, the SC array (an inside array) works best for the shallow and intermediate-depth portions of the models (region where the model is constrained by data). This contradicts conventional wisdom that inside arrays are worse for vertical boundaries, [e.g. Ward, 1990; Reynolds, 1997]. For the vertical conductor (VLL), the outside arrays perform better than the inside arrays, which fail for the intermediate-depth to deep portions of the model, in accordance with conventional wisdom, [e.g. Ward, 1990; Reynolds, 1997]. The

polarity change of the layer from a resistor to a conductor changed array performance from an inside array performing best to an outside array.

For the horizontal conductor over resistor model (HBL), the outside arrays perform better than the inside arrays for the intermediate-depth and deep portions of the model (Appendix C). Again, this contradicts conventional wisdom that outside arrays are worse for horizontal boundaries, [e.g. Ward, 1990; Reynolds, 1997]. For the horizontal resistor over conductor model (HBH), the inside arrays perform slightly better than the outside arrays for the intermediate-depth and deep portions of the model, in accordance with conventional wisdom. Again, the polarity change from a conductive to a resistive layer changed array performance from an inside array performing best to an outside array. For the undulating boundary model (UB), the DD, PD and SC arrays perform equally well. The good performance of the outside arrays contradicts conventional wisdom, [e.g. Ward, 1990; Reynolds, 1997]. The greatest mismatch is near the resistivity boundary for all three models.

For the horizontal conductive (HLL) and resistive layer models (HLH), the DD array best matches the resistivity of the layer (Appendix C). However, all arrays poorly quantify the resistivity of the thin layer, especially for the resistive layer surrounded by conductors. The greatest mismatch is near the resistivity boundaries and is worse for the deeper boundary in both models. For the HLL model, all arrays perform acceptable to well in the shallow portion and well in the deep portion of the model. For the HLH model, all arrays perform well in the shallow and deep portions of the model, except the PP that is acceptable in the shallow and poor in the deep. The good performance of the

outside arrays contradicts conventional wisdom that outside arrays are worse for horizontal boundaries.

For the dipping conductive (DLL) and resistive layer models (DLH), all arrays perform well in the shallow portion of the models (Appendix C). All arrays fail for the deep portion of the DLL and the intermediate-depth portion of the DLH model. For the DLL model, the DD performs well in the intermediate-depth, the WN fails, and the remaining arrays perform acceptably. For the DLH model, the WN performs well in the deep, the two- and three-pole arrays fail, and the remaining arrays perform acceptably.

For the conductive block model (BL), all arrays perform well throughout the model, except the PP that is acceptable for the intermediate-depth portion of the model (Appendix C). For the resistive block model (BH), all arrays perform well throughout the model. The greatest mismatch is near the boundaries and is worse for the deeper boundaries in both models. Since the block models are a combination of horizontal and vertical boundaries, there is no conventional wisdom for which array is best.

Table 9 shows the overall array performance grades based on the resistivity mismatches for all twelve models used in this study. The DD and PD arrays do not fail for any model and perform well for most models, the DD holds a slight advantage when comparing acceptable array performance. The SC and PP arrays each fail for one model and frequently perform well for the remaining models with the SC holding a slight advantage. The WN fails for three models and frequently performs well for the remaining models.

For the VB model, all arrays perform equally well (Table 9). For the VLL model, the outside arrays perform best. For the VLH, HBL, HBH, and UB models, all arrays

perform well. For the HLL model, the four- and three-pole outside arrays perform best. For the HLH model the four- and three-pole arrays perform acceptably. For the DLL and DLH models, none of the arrays are good, but acceptable arrays are the four- and three-pole arrays. For the BL model, the best arrays are the four- and three-pole arrays. For the BH model, the best arrays are the four- and three-pole outside and SC arrays.

The resistivity mismatch (Appendix C) shows that all arrays perform well and nearly equally for the shallow portion of the models, with a few exceptions. For all models the greatest mismatch in resistivity is near the discontinuities in the model. When resistivity boundaries exist in the deep portion of the models, the resistivities are poorly reproduced. Field surveys must be designed so that the geologic target is in the shallow to intermediate-depth range and in the middle of the data constrained region of Figure 2.

Table 9 shows that a polarity change between conductor and resistor resulted in a change in array performance for some models. This implies that the distribution of resistivities is equally important as the boundary geometries for determining the optimal array for the particular geologic situation under investigation. The DD and PD arrays do not fail for any model and frequently receive high grades. Therefore, these arrays are recommended if no prior information is known about the geology at a site. The optimal array for a particular field area can only be decided once some geologic information is gained through preliminary field reconnaissance or onsite testing during fieldwork.

Boundary Mismatch

The combined boundary mismatch for the vertical boundary model (VB) shows that all arrays perform well in the shallow and intermediate-depth portions of the model (Table 7). Four-pole arrays perform equally well in the deep portion of the model. The

good performance of the inside arrays contradicts conventional wisdom which states that inside arrays are worse for vertical boundaries [e.g. Ward, 1990; Reynolds, 1997].

For the vertical conductor model (VLL), all arrays perform well in the shallow portion of the model, except the WN that fails throughout the model (Appendix F). Outside arrays perform well in the intermediate-depth portion of the model, while the inside arrays fail in the intermediate-depth and deep portions of the model. The DD performs well, the PP acceptably, and the PD fails in the deep portion of the model; these three arrays find the layer but make it too wide. For the vertical resistor model (VLH), all arrays perform well in the shallow and intermediate-depth portions of the model (Appendix F). All arrays fail in the deep portion of the model. The good performance of the inside arrays contradicts conventional wisdom, which states that inside arrays are worse for vertical boundaries [e.g. Ward, 1990; Reynolds, 1997]. The polarity change of the vertical layer from a conductor to a resistor changed array performance from an outside array performing best to the inside arrays.

For the horizontal conductor over resistor model (HBL) and the horizontal resistor over conductor model (HBH), the outside arrays perform well throughout the model (Appendix F). The inside arrays perform acceptably for the HBL, finding the boundary too deep and wide. All arrays perform well for the HBH and undulating boundary (UB) models, except the WN that performs only acceptably for the UB. All arrays resolve the boundary in the UB model too wide and the WN locates it too deep as well. The good performance of the outside arrays and relatively poor performance of the inside arrays for the HBL and UB models contradicts conventional wisdom, which states that inside are best and outside arrays are worse for resolving horizontal boundaries, [e.g. Ward, 1990;

Reynolds, 1997]. When the polarity of the upper layer is changed from conductive to resistive, array performance for the inside array goes from acceptable to good.

For the horizontal conductor in a resistor (HLL) and resistor in a conductor (HLH) models, the DD array performs well for the shallow and the SC performs acceptably (Appendix F). The WN array fails for the entire HLL model. The outside arrays perform acceptably, while the inside arrays fail for the intermediate-depth portion of the HLL model, resolving the lower boundary too deep and wide. The WN array resolves the upper boundary for the HLL shallower than it should. All arrays perform acceptably in the intermediate-depth portion of the HLH model, except the PP that fails. All arrays resolve the layer thicker than it should be. The good performance of the DD and relatively poor performance of the inside arrays contradicts conventional wisdom. Again, a change in the polarity of the layer changed array performance; the inside arrays fail for the conductor but are acceptable for the resistor.

For the dipping conductor (DLL) and dipping resistor (DLH) models, all arrays perform well in the shallow portion of the model (Appendix F). The three-pole array performs acceptably in the intermediate-depth portion of both models and the remaining arrays fail. All arrays fail in the deep portion of the models. The good performance of the outside arrays contradicts conventional wisdom.

For the conductive block model (BL), all arrays perform well throughout the model, except the SC that is acceptable in the deep and the PP that fails in the intermediate-depth and deep (Appendix F). For the resistive block model (BH), the DD, PD and SC arrays perform well in the shallow and acceptably in the intermediate-depth portions of the model. The PP performs acceptably in the shallow, where the WN array

fails, and both arrays fail for the intermediate-depth portion of the model. The DD performs well in deep portion of the models while all of the remaining arrays fail. The change in polarity of the block changed array performance; the inside arrays and the three-pole array perform better for the BL model than the BH model.

Table 10 shows the overall array performance grades based on the combined boundary mismatch for all twelve models used in this study. The PD array does not fail for any model, but also does not receive many A grades and is frequently only acceptable. The DD only fails for one model and frequently receives A grades. The SC fails for three models and performs well to acceptable for the remaining models. The PP fails for five models and performs well for six out of the remaining seven models. The WN fails for five models and performs well for three of the remaining seven models. The overall array performance grades seem to correlate with the number of data points for each array, PD (1771), DD (1375), SC (1048), PP (664) and finally WN (392). However, for the VB, VLH, HBH, and UB models array performance is nearly equivalent (Table 10). The WN array, 392 data points, receives A's and B's for the VB, VLH, HBH, and BL models. For the VLH model the dipole-dipole, 1375 data points, receives a C. Other similar patterns can be seen in Table 10 showing that array performance is specific to model geometries and resistivity distributions and not strictly related to the number of data points.

For the VB model, the four-pole arrays perform the best (Table 10). For the VLL, HBL, and UB models the outside arrays perform best. For the VLH model, the inside and two- and three-pole arrays perform best. For the HBH model, all arrays perform well. For the HLL model, the four- and three-pole outside arrays perform best. For the HLH and

BL models, the four- and three-pole arrays perform well. For the DLL model, none of the arrays are good, but acceptable arrays are the four- and three-pole outside and the SC. For the DLH model, none of the arrays are good, but acceptable arrays are the two- and three-pole outside arrays. For the BH model, the best arrays are the four- and three-pole outside and the SC arrays.

Boundaries in the deep portion of the models are not well reproduced by any of the arrays (Appendix F). Field surveys must be designed so that the geologic target is in the shallow to intermediate-depth range and in the middle of the data constrained region of Figure 2. These mismatches also show that polarity change between high and low resistances in a model often results in a change in array performance at reproducing model boundaries. This implies that the distribution of resistivities is equally important as the boundary geometries for determining the optimal array for the particular geologic situation under investigation.

The DD and PD arrays rarely fail for any model and frequently receive high grades (Table 10). Therefore, these arrays are recommended if no prior information is known about the geology at a site. The optimal array for a particular field area can only be decided once some geologic information is gained through preliminary field reconnaissance or onsite testing during fieldwork.

Synthesis

All arrays have small resistivity mismatches for the shallow portion of the models, and with a few exceptions perform nearly equally (Appendices B & C). For all arrays, the greatest mismatch in resistivity is near the discontinuities in the models and the resistivities are poorly reproduced in the deep portion of the models. Boundaries in

the deep portion of the models are not well reproduced by any of the arrays (Appendices D, E, & F). Field surveys must be designed so that the geologic target is in the shallow to intermediate-depth range and in the middle of the data constrained region of Figure 2.

Changing the polarity of geologic units from resistors to conductors often changes relative array performance at reproducing model resistivities and boundary geometries (Tables 9 & 10). This implies that both the distribution of resistivities and the boundary geometries need to be considered in determining the optimal array for the geologic situation under investigation. For the vertical resistive layer, the Schlumberger array performs best at reproducing model resistivities and boundary geometries. When the polarity of the vertical layer is changed from a conductor to a resistor, the outside arrays perform better. For the horizontal conductor over resistor, the inside arrays perform well at reproducing model resistivities and boundary geometries. When the polarity is changed to resistor over conductor, the performance of the inside arrays declines and the outside arrays performer better. For the horizontal resistive layer, the inside arrays fail at reproducing model boundary geometries. When the polarity of the layer is changed from a resistor to a conductor, the performance of the inside arrays becomes acceptable. For the resistive block, the three-pole and inside arrays reproduce the model boundary marginally. When the polarity of the block is changed from a resistor to a conductor, the performance of these arrays improves. The change in array performance for different polarities is likely to be caused by the distribution of current in the subsurface. Current becomes concentrated in conductors and diffused in resistors. Each array has a different sensitivity to changes in the current distribution and as a result array performance changes.

One unexpected result is the poor performance of all arrays for resolving the dipping structures. Li and Oldenburg (2000) investigated the incorporation of known geologic dip information into the inversion. They concluded that an optimization method with smoothing parallel to geologic dip has higher resolution and provides a better representation of the true structure. The results of the dipping structure models may be improved by applying this inversion optimization method to the data sets from this study.

Conclusions and Recommendations

Previous studies of the relative performance of standard electrode arrays for various geologic situations have resulted in conventions and tables of applicability of each array [e.g., Ward, 1990; Reynolds, 1997; Sharma, 1997]. These conventions are based upon labor intensive field operations, 1D vertical sounding or horizontal profiling, and semi-quantitative dataanalysis based on master curve fitting of apparent resistivity or trial-and-error pseudosection matching. Modern systems allow efficient 2D data acquisition, combining sounding and profiling. Improvements in computing technology have allowed 2D inversion of resistivity data to become the primary method of determining subsurface resistivity structure. Yet, the conventions based upon 1D studies are still the basis for array selection for modern surveys. Table 10 replaces the previous conventions with array performance based upon modern acquisition and analysis techniques.

Although in some cases, we corroborate conventional wisdom, several findings contradict conventional wisdom. These differences are likely due to the use of 2D data, combining sounding and profiling, and the use of 2D inversion modeling. Inversion modeling obtains a 2D subsurface resistivity structure for comparison to the true model

rather than simply comparing apparent resistivity profiles, soundings, and pseudosections. In addition to testing a wider range of simple models than past studies, this study looks at resistivity mismatch as a function of depth, depth dependent recovery of the position and width of discontinuities, and the effect of reversing the polarity of geologic units.

Although the synthetic, noise-free data were well matched for all inversions, many of the inversion results exhibit substantial mismatches from the true model. Since the data misfit is the only criterion currently available for real data, practitioners need to realize that the inversion result represents the subsurface with a lesser degree of accuracy than the apparent resistivity data misfit.

When resistivity boundaries exist in the deep portion of the models, the resistivities of geologic units and the position and width of geologic boundaries are not well reproduced by any array. The poor performance of all arrays at reproducing resistivities and boundaries in the deep portions of the models shows that field surveys must be designed so that the geologic target is in the shallow to intermediate-depth range and in the middle of the data constrained region (Figure 2).

The primary criterion for array performance in this study is reproduction of geologic boundaries. When multiple arrays receive the same grade, a second criterion (the number of data points necessary to obtain the results or a slightly better resolution of position and width of geologic boundaries) could be used to decide the optimal array choice. Different arrays performed best for different model geometries and a practical table (Table 10) was presented to allow the practitioner to choose the optimal array for the geologic situation under investigation. Changing the polarity of geologic units from

resistors to conductors in fixed model geometries often affected array performance. The distribution of resistivities is equally important as the model geometries, for determining the optimal array for the particular geologic situation under investigation. Pre-investigation of an area should be undertaken to determine the geometry of the geologic boundaries and the distribution of resistivities. Although the DD and PD arrays may not be the optimal array for a given geology, they rarely fail for any model, and thus are recommended for reconnaissance or onsite testing during fieldwork. Multi-channel systems would make onsite investigation during fieldwork feasible as collection of multiple electrode combinations could be completed in a very short time period. The optimal array choice for a particular field site can then be determined from Table 10 once the geometry of geologic boundaries and the distribution of resistivities are determined.

References

Barker, R. D., 1989, Depth of investigation of collinear symmetrical four-electrode arrays: Geophysics, vol. 54 p. 1031-1037.

Barker, R. D., 1992, A simple algorithm for electrical imaging of the subsurface: First Break, vol. 10 p. 53-62.

Beard, L. P. & Tripp A. C., 1995, Investigating the resolution of IP arrays using inverse theory: Geophysics, vol. 60, p. 1326-1341.

Coggon, J. H., 1973, A Comparison of IP Electrode Arrays: Geophysics, vol. 38, p.737-761.

Dahlin, T., 1996, 2D resistivity surveying for environmental and engineering applications. First Break vol. 14 p. 275-283.

Dahlin, T. & Loke, M. H., 1998, Resolution of 2D Wenner resistivity imaging as assessed by numerical modelling: Journal of Applied Geophysics, vol. 38, p. 237-249.

Dahlin, T. & Zhou, B., 2004, A numerical comparison of 2D resistivity imaging with 10 electrode arrays: Geophysical Prospecting, vol. 52, p. 379-398.

Dey, A., Meyer, W. H., Morrison, H. F. & Dolan, W. M., 1975, Electric field response of two-dimensional inhomogeneities to unipolar and bipolar electrode configurations: Geophysics, vol. 40, p. 630-640.

Dey, A. and Morrison, H. F., 1979, Resistivity Modelling for Arbitrary Shaped Two-Dimensional Structures: Geophysical Prospecting, vol. 27, p. 106-136.

Edwards, L. S., 1977, A modified pseudosection for resistivity and IP: Geophysics, vol. 42, p. 1020-1036.

Ellis, R. G. and Oldenburg, D. W., 1994, Applied geophysical inversion: Geophys. J. Int., vol. 116, p. 5-11.

Ellis, R. G. and Oldenburg, D. W., 1994, The pole-pole 3-D DC resistivity inverse problem: a conjugate gradient approach: Geophys. J. Int., vol. 119, p.187-194.

Griffiths, D. H. & Turnbull, J., 1985, A multi-electrode array for resistivity surveying: First Break, vol. 3, p. 16-20.

Griffiths, D. H., Turnbull, J. & Olayinka, A. I., 1990, Two-dimensional resistivity mapping with a computer controlled array: First Break, vol. 8, p. 121-129.

Griffiths, D.H. & Barker, R.D., 1993, Two-dimensional resistivity imaging in areas of complex geology: Journal of Applied Geophysics, vol. 29, p. 211-226.

Li, Y. and Oldenburg, D. W., 1992, Approximate inverse mappings in DC resistivity problems: Geophysical Journal International, vol. 109, p. 343-362.

Li, Y. and Oldenburg, D. W., 1994, Inversion of 3-D DC resistivity data using an approximate inverse mapping: Geophys. J. Int., vol.116, p. 527-537.

Li, Y. and Oldenburg, D. W., 2000, Incorporating geological dip information into geophysical inversions: Geophysics, vol.65, p. 148-157.

Loke, M. H. and Barker, R. D., 1995, Least-squares deconvolution of apparent resistivity pseudosections: Geophysics, vol. 60, p. 1682-1690.

Loke, M. H., & Barker, R.D., 1996, Rapid least squares inversion of apparent resistivity pseudosections by a quasi-Newton method: Geophysical Prospecting, vol. 44, p. 131-152.

Loke, M. H., 2002, Manual for RES2DMOD ver. 3.01q: Rapid 2D-resistivity forward modeling using the finite-difference and finite-element methods.

Loke, M. H., 2002, Manual for RES2DINV ver. 3.51z: Rapid 2D-resistivity & IP inversion using the least squares method.

Loke, M. H., Acworth, I. & Dahlin, T., 2003, A comparison of smooth and blocky inversion methods in 2D electrical imaging surveys: Exploration Geophysics, vol. 34, p. 182-187.

McGillivray, P. R., Oldenburg, D. W., Ellis, R. G. & Habashy, T. M., 1994, Calculation of sensitivities for the frequency-domain electromagnetic problem: Geophysical Journal International, vol. 116, p. 1-4.

Oldenburg, D. W., 1978, The interpretation of direct current resistivity measurements: Geophysics, vol. 43, p.610-625.

Oldenburg, D. W. and Li, Y., 1999, Estimating depth of investigation in dc resistivity and IP surveys: Geophysics, vol. 64, p. 403-416.

Pain, C. C., Herwanger, J. V., Worthington, M. H. & de Oliveira, C. R. E., 2002, Effective multidimensional resistivity inversion using finite-element techniques: Geophysical Journal International, vol. 151, p. 710-728.

Park, S. K. and Van, G. P., 1991, Inversion of pole-pole data for 3-D resistivity structure beneath arrays of electrodes: Geophysics, vol. 56, p. 951-960.

Pratt, D. A. & Whiteley, R.J., 1974, Computer simulation and evaluation of electrode array responses in resistivity and IP prospecting: Bulletin of the Australian Society of Exploration Geophysics, vol. 5, no. 2, p. 65-87.

Robain, H., Albouy, Y., Dabas, M., Descloitres, M., Camerlynck, C., Mechler, P. & Tabbagh, A., 1999, The location of infinite electrodes in pole-pole electrical surveys: consequences for 2D imaging: Journal of Applied Geophysics, vol. 41, p. 313-333.

Roy, A. & Apparao, A., 1971, Depth of investigation in direct current methods: Geophysics, vol. 36, p. 943-959.

Sasaki, Y., 1992, Resolution of resistivity tomography inferred from numerical simulation: Geophysical Prospecting, vol. 40, p. 453-463.

Seaton, W. J. and Burbey, T. J., 2002, Evaluation of two-dimensional resistivity methods in a fractured crystalline-rock terrane: Journal of Applied Geophysics, vol. 51, p. 21-41.

Sharma, P. V., 1997, Environmental and engineering geophysics, pp. 207-264. Cambridge, UK: Cambridge University Press.

Stummer, P, Maurer, H. & Green, A., 2004, Experimental design: Electrical resistivity data sets that provide optimum subsurface information: Geophysics, vol. 69, p. 120-139.

Sumner, J.S., 1976, Principles of induced polarization for geophysical exploration, Elsevier Publishing company.

Telford, W.M., Geldart, L.P., & Sheriff, R.E., 1990, Applied Geophysics, pp. 522-577. Cambridge, UK: Cambridge University Press.

Ward, S. H., 1990, Resistivity and IP Methods in Geotechnical and Environmental Geophysics Vol. 1: Society of Exploration Geophysicists, Investigations in Geophysics.

Whiteley, R.J., 1973, Electrode arrays in resistivity and IP prospecting: a review: Bulletin of the Australian Society of Exploration Geophysics, vol. 4, p. 1-29.

Zhou, B. & Greenhalgh, S. A., 2000, Cross-hole resistivity tomography using different electrode configurations, Geophysical Prospecting, vol. 48, p. 887-912.

Model name	Geologic possibilities
Vertical Boundary (VB)	Discrete fault, contact, unconformity
Vertical Layer Low (VLL)	Saturated or conductively mineralized fault zone
Vertical Layer High (VLH)	Dry fault zone, lithology change
Horizontal Boundary Low (HBL)	Dry soil over bedrock, water table in soil or bedrock
Horizontal Boundary High (HBH)	Moist over dry soil, moist soil over bedrock, perched water table
Undulating Boundary (UB)	Change in layer thickness or depth to bedrock
Horizontal Layer Low (HLL)	Dry soil/moist soil/bedrock, perched water table, saturated fracture zone
Horizontal Layer High (HLH)	Moist soil/dry soil/water table, perched water table, dry fracture zone
Dipping Layer Low (DLL)	Saturated or conductively mineralized fault zone, lithology change
Dipping Layer High (DLH)	Dry fault zone, lithology change
Block Low (BL)	Mineral deposit, water filled void or tunnel
Block High (BH)	Air filled void or tunnel

Table 1 – Geologic possibilities for the models used in this study.

Array	Max a-spacing	Max n-spacing	Number of data points	Min pseudodepth	Max pseudodepth
DD	16	6	1375	0.42	10.4
PD	16	6	1771	0.52	17.3
PP	16		664	0.87	13.9
WN	16		392	0.51	8.2
SC	16	6	1048	0.52	9.2

Table 2 – Array spacings, number of data points, and maximum and minimum pseudodepths for each array for a fixed 50-electrode multi-core cable. Spacings and pseudodepths are dimensionless.

Array	Data RMS (%)	Model RMS (%)	Rank
DD	0.13	4.58	1st
PD	0.20	14.82	2nd
PP	0.24	19.34	4th
WN	0.23	25.61	5th
SC	0.12	15.43	3rd

Table 3 – Data misfit and model mismatch statistics and relative array rank based on the model mismatch statistics (units are %) for the vertical boundary model. Array acronyms from Figure 1.

	Resistivity Mismatch			Performance Grade			Final
Array	S	I	D	S	I	D	Grade
DD	2.06	1.84	6.27	A	A	A	A
PD	3.06	5.97	21.07	A	A	B	A
PP	3.14	10.72	31.34	A	A	B	A
WN	3.19	14.79	41.16	A	A	C	B
SC	1.71	1.38	22.76	A	A	B	A

Table 4 – Resistivity mismatches and array performance grades for the shallow (S), intermediate-depth (I), and deep (D) portions of the vertical boundary model, and overall array performance grade for all arrays. Array acronyms from Figure 1.

	Position Mismatch			Performance Grade		
Array	S	I	D	S	I	D
DD	0.00	0.00	0.00	A	A	A
PD	0.00	0.83	9.25	A	A	B
PP	0.00	2.92	14.83	A	A	C
WN	0.00	0.00	0.00	A	A	A
SC	0.00	0.00	0.00	A	A	A

Table 5 – Mean normalized position mismatches and array performance grades for the S, I, and D portions of the vertical boundary model. Depth acronyms from Table 4. Array acronyms from Figure 1.

	Width Mismatch			Performance Grade		
Array	S	I	D	S	I	D
DD	0.00	0.00	0.98	A	A	A
PD	0.00	0.67	11.84	A	A	C
PP	0.00	2.44	14.58	A	A	C
WN	0.00	0.44	1.98	A	A	A
SC	0.00	0.00	0.00	A	A	A

Table 6 – Mean normalized width mismatches and array performance grades for the S, I, and D portions of the vertical boundary model. Depth acronyms from Table 4. Array acronyms from Figure 1.

	Combined Position & Width			Performance Grade		
Array	S	I	D	S	I	D
DD	0.00	0.00	0.64	A	A	A
PD	0.00	0.72	10.94	A	A	C
PP	0.00	2.61	14.67	A	A	C
WN	0.00	0.29	1.29	A	A	A
SC	0.00	0.00	0.00	A	A	A

Table 7 –Combined mean boundary mismatches and array performance grades for the S, I, and D portions of the vertical boundary model. Depth acronyms from Table 4. Array acronyms from Figure 1.

Array	Overall Grade
DD	A
PD	B
PP	B
WN	A
SC	A

Table 8 – Overall array performance grades based on the combined boundary mismatches for the vertical boundary model (Table 7). Array acronyms from Figure 1.

	VB	VLL	VLH	HBL	HBH	UB	HLL	HLH	DLL	DLH	BL	BH
DD	A	B	B	B	B	B	B	C	C	C	A	A
PD	A	C	B	B	B	B	B	C	C	C	A	A
PP	A	B	B	B	B	B	C	E	C	C	B	B
WN	B	E	B	B	B	B	C	C	D	D	A	B
SC	A	D	B	B	B	B	C	C	C	C	A	A

Table 9 - Overall array performance grades based on the resistivity mismatches for all twelve models used in this study. (no shading = good array performance; light grey shading = acceptable array performance; dark grey shading = poor array performance. Array acronyms from Figure 1, Model Acronyms from Table 1.)

	VB	VLL	VLH	HBL	HBH	UB	HLL	HLH	DLL	DLH	BL	BH
DD	A	A	C	A	A	B	B	B	C	D	A	B
PD	B	B	B	B	A	B	C	C	C	C	A	C
PP	B	B	B	B	A	B	D	E	D	C	D	D
WN	A	E	B	C	A	C	D	C	D	D	A	E
SC	A	D	B	C	A	B	D	C	C	D	B	C

Table 10 – Overall array performance grades based on the combined boundary position and width mismatches for all twelve models used in this study. (no shading = good array performance; light grey shading = acceptable array performance; dark grey shading = poor array performance. Array acronyms from Figure 1, Model Acronyms from Table 1.)

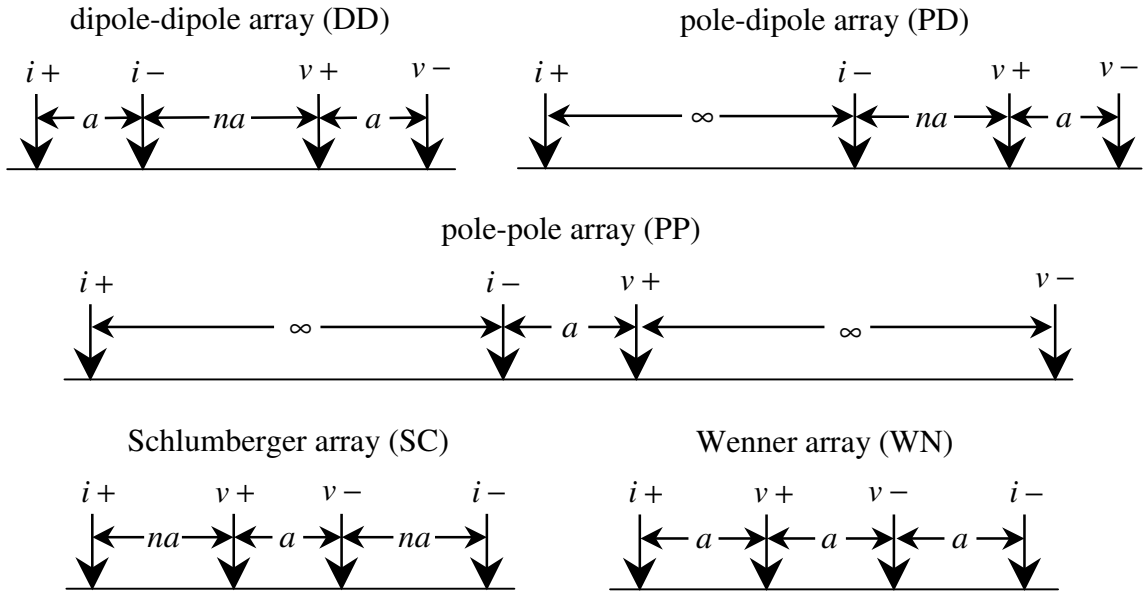

Figure 1 – Schematic diagram of the five DCR arrays used in this study illustrating current (*i*) and potential (*v*) electrodes. "*a*" is a distance, which is restricted in multi-electrode cabled systems to an integer number of electrode spacings. "*n*" is an integer multiplier. The values of *a* and *n* used in this study are given in Table 2.

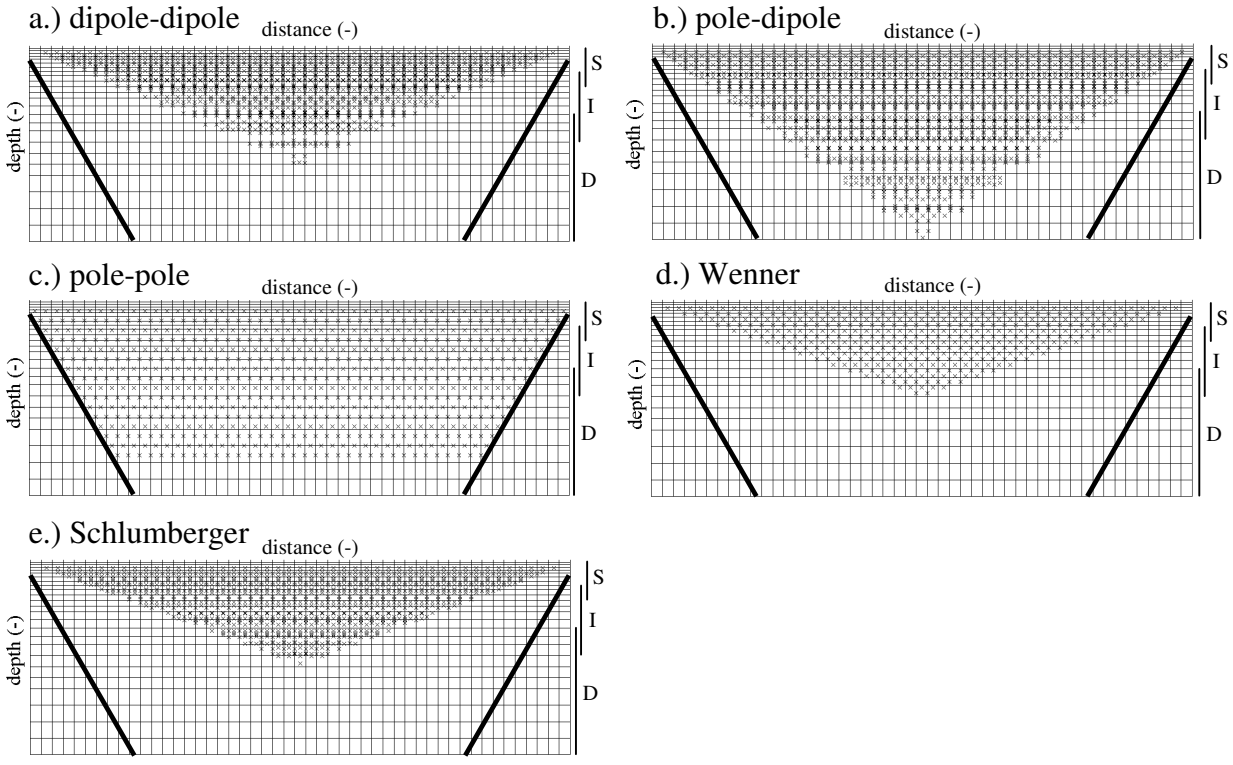

Figure 2 – The arrangement of finite difference model blocks and location of the midpoint and pseudodepth of datum points (X) for the five arrays. Triangular region between the black lines and the model edges indicate the region truncated when comparing inversion results to the true model. The arbitrary definitions of shallow (S), intermediate-depth (I) and deep (D) are shown. Distance and depth are dimensionless.

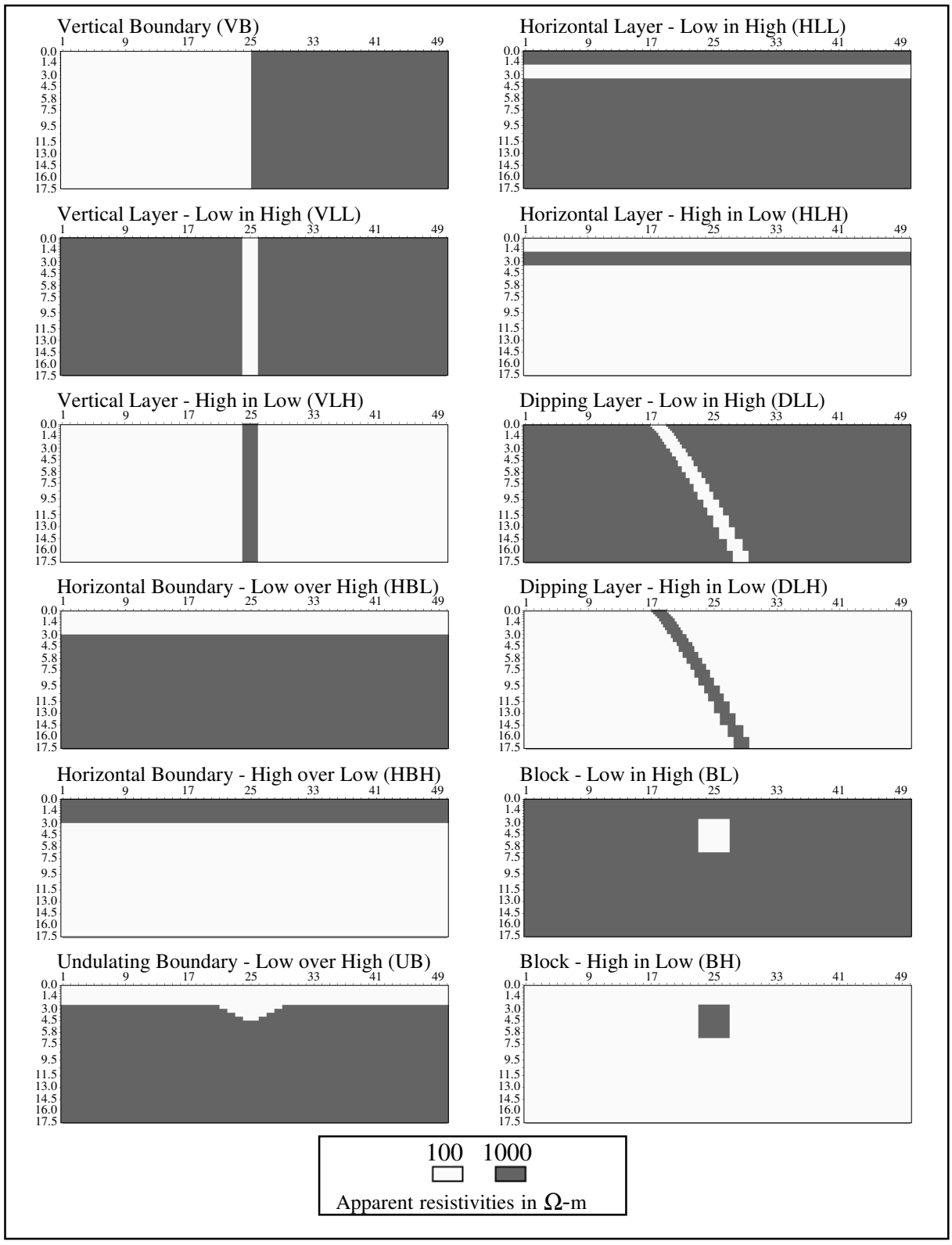

Figure 3 – The twelve geologic models used in this study. High represents a resistor and Low represents a conductor. The horizontal axis is distance and the vertical axis is depth, both axes are dimensionless.

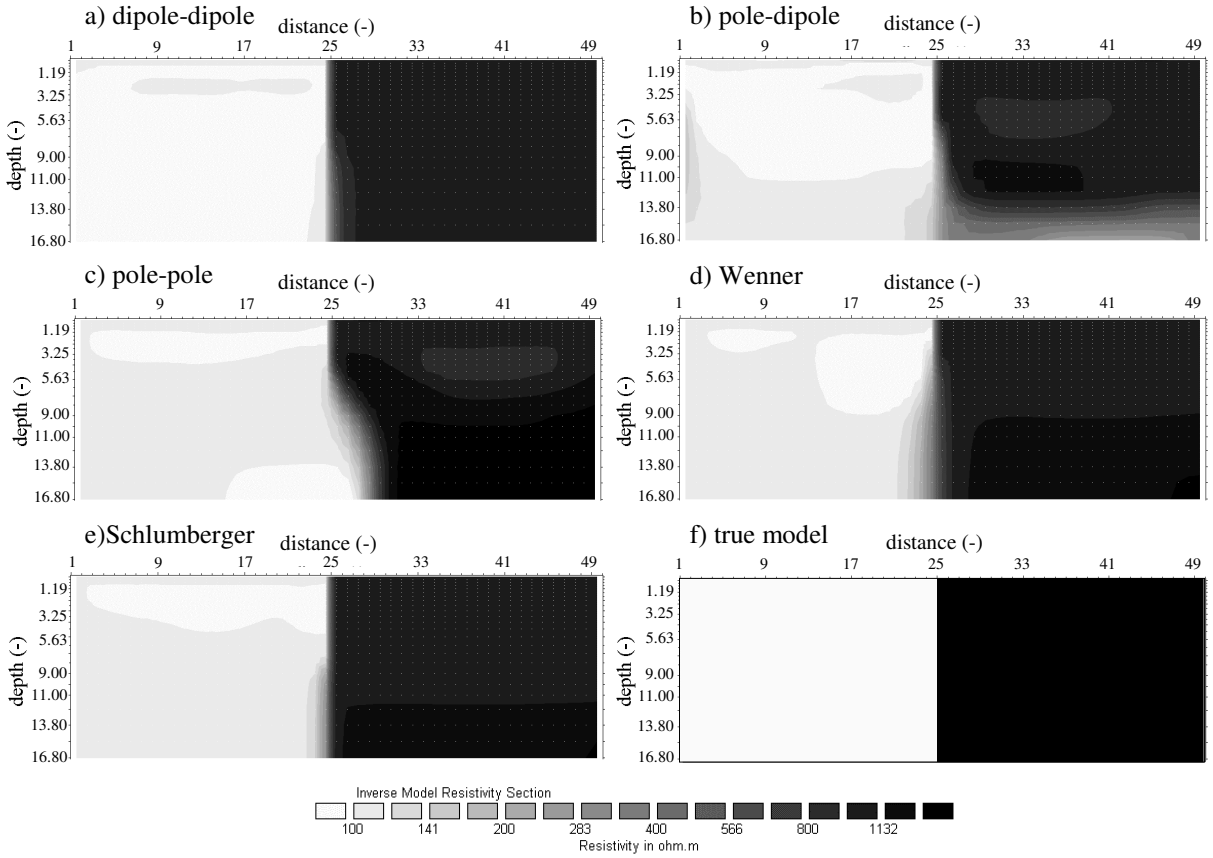

Figure 4 – Inversion results for the vertical boundary model using the data from the; a) dipole-dipole, b) pole-dipole, c) pole-pole, d) Wenner, and e) Schlumberger arrays. The true model (f) is included for comparison. Distance and depth are dimensionless.

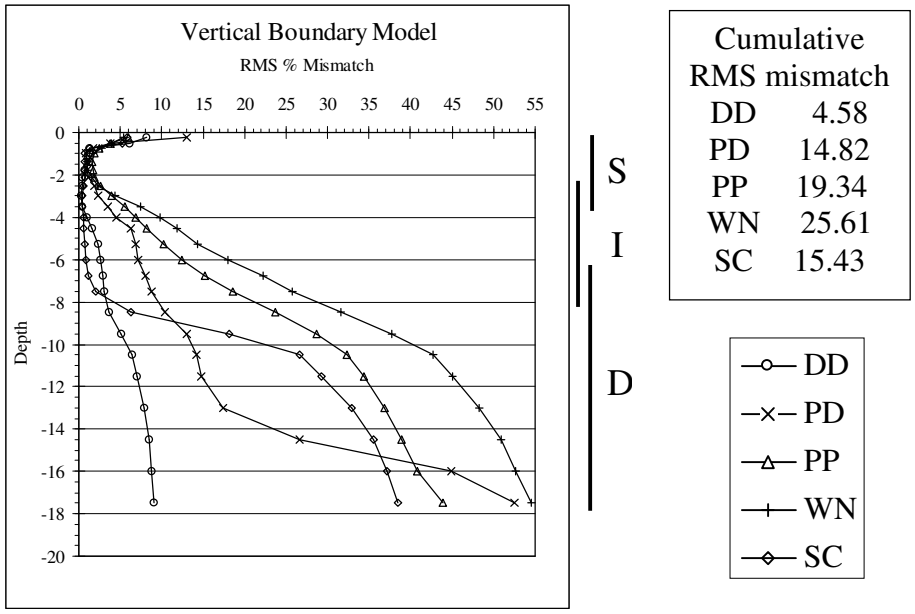

Figure 5 – Graph of the layer-by-layer resistivity mismatch and Table of cumulative resistivity mismatch for the five DCR arrays for the vertical boundary model. The arbitrary definitions of shallow (S), intermediate-depth (I), and deep (D) are shown. Array acronyms are the same as Figure 1.

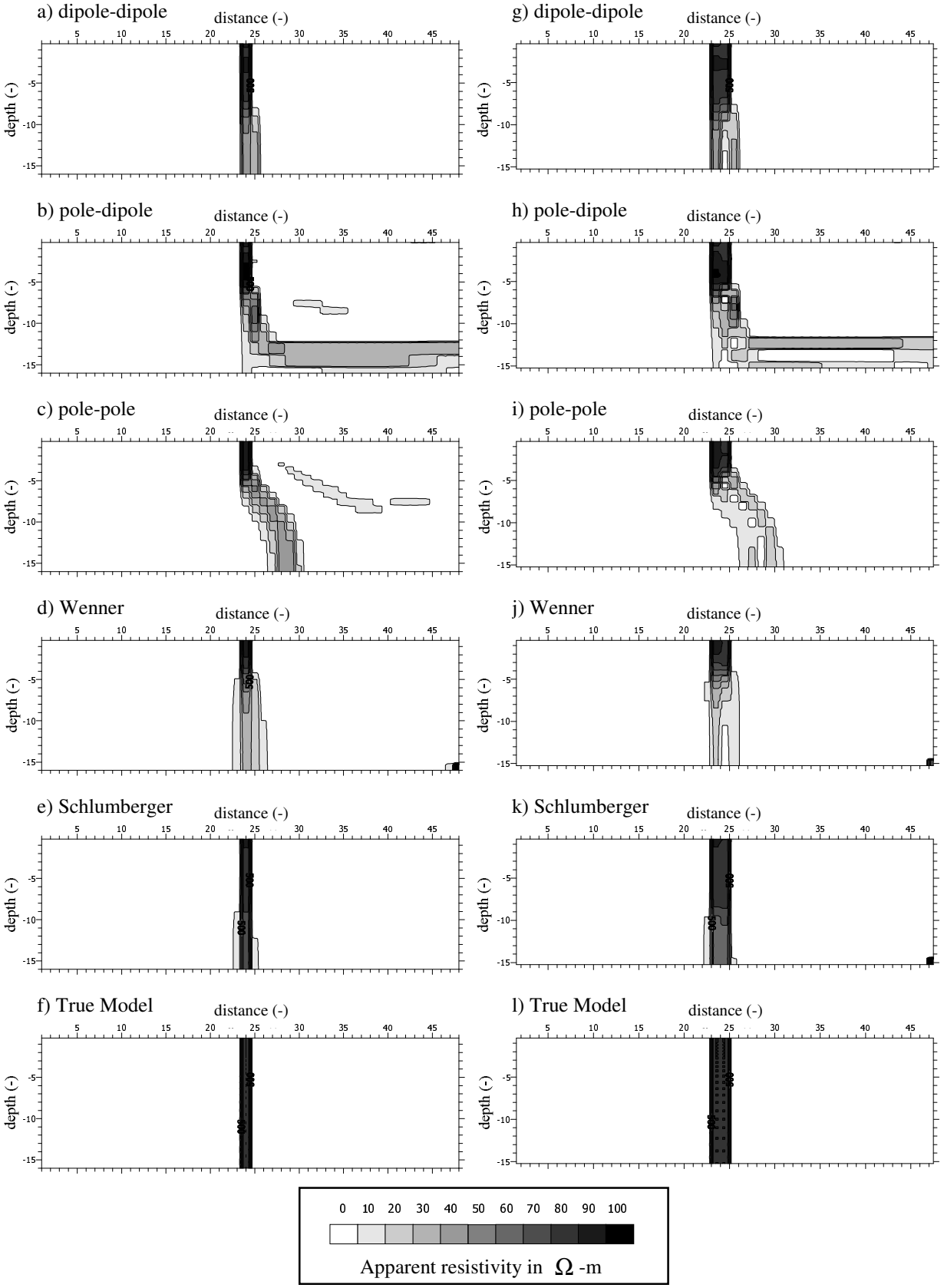

Figure 6 – Plots of the spatial gradient (left) and spatial Laplacian (right) of the inversion results of Figure 4 for the five DCR arrays and the true model. Distance and depth are dimensionless.